ISSN: 2754-4753

Journal of Physics & Optics Sciences

Review Article

Open Access

Modelling of a Binary System with a Quadratic Equation of State

Manuel Malaver[1,2]* and Rajan Iyer[3]

[1]Department of Basic Sciences, Maritime University of the Caribbean, Catia la Mar, Venezuela

[2]Institute of Scholars, Muddhinapalya Bengaluru-560091, Karnataka, India

[3]Environmental Materials Theoretical Physicist, Department of Physical Mathematics Sciences Engineering Project Technologies, Engineeringinc International Operational Teknet Earth Global, Tempe, Arizona, United States of America

ABSTRACT

This study investigates Einstein-Maxwell field equations with anisotropic pressure by means of a quadratic equation of state (Bose-Einstein equation of state) in the presence of an electric field and a modified version of the metric potential proposed for Korkina and Orlyanskii (1991). We obtain new classes of models that satisfy all the physical conditions for a realistic star. According to visual analysis, physical properties including energy density, radial pressure, charge density, and anisotropy are consistent with the stellar binary system GW191219, which is composed of a neutron star and a black hole.

***Corresponding author**

Manuel Malaver de la Fuente, Department of Basic Sciences, Maritime University of the Caribbean, Catia la Mar, Venezuela.

Received: March 12, 2025; **Accepted:** March 22, 2025; **Published:** April 07, 2025

Keywords: Einstein-Maxwell Equations, Anisotropic Pressures, Quadratic Equation of State, Anisotropy, Binary System

Introduction

Einstein's general theory of relativity (GR) is regarded as a foundational theory for comprehending the structure and behavior of stellar heavy objects, including as white dwarfs, pulsars, quasars, and neutron stars [1,2]. Karl Schwarzschild conducted the first theoretical investigation in GR in 1916 when he discovered a universal vacuum external solution [3]. Additionally, Einstein provides significant contributions to the study of the universe's structure, leading to pertinent developments in cosmology and astrophysics [4].

For many years, it was believed that the interior of stars was ideal, with equal tangential (p_t) and radial (p_r) pressures, which results in the isotropic local condition $p_r = p_t$ [5]. However, theoretical research on actual star models by Ruderman and Canuto suggest that the nuclear matter can present anisotropy in high density ranges (ρ > 1015 g/ cm3) [6,7]. The radial and tangential pressures in large objects are different, and a solid core, phase transitions, magnetic fields, and pion condensation can all cause anisotropy in the pressures [8,9]. According to Usov, pressure anisotropy may also be brought on by a powerful electric field [10]. Bowers and Liang examined an anisotropic fluid model in their groundbreaking work and came to the conclusion that anisotropy affected the maximum equilibrium mass and surface redshift [10]. Additionally, in order to integrate having analytical solutions with the Einstein field equations, Dev and Gleiser have proposed an equation that links the radial and tangential pressures and have offered new exact solutions for the distribution of matter with tangential pressures and uniform energy density [8]. The impact of anisotropy on the physical characteristics of a matter distribution in relativistic compact objects has been examined by researchers such as Cosenza et al., Bayin, Krori et al., Herrera and Ponce de León, Ponce de León, Bondi, Herrera and Santos, Herrera et al., Dev and Gleiser, Ivanov, Mak and Harko, Mak et al., Viaggiu, Malaver, and Pant et al. [11-35].

In a groundbreaking treatment, it was initially hypothesized that weird quark stars might exist in hydrostatic equilibrium for Itoh [36]. According to the strange quark matter concept, there are an equal number of up and down quarks in the quark matter, and the strange quarks can be thought of as the absolute ground state for the hadron confined state [37]. Strange stars are not included in equilibrium configurations like neutron stars and white dwarfs because it is now known that they arise when the center of a large object collapses following a supernova explosion.

The fact that weird stars are self-bound by a strong interaction—gravity only makes them massive—while neutron stars are bound by gravity is a key difference between them and regular neutron stars. Because of this, a weird star can rotate more quickly than a neutron star could. The surface electric fields associated with a strange star are the most intriguing difference between it and a typical neutron star. The ultra-strong electric fields found on the surface of strange stars are around 1018 V/cm for regular strange matter and 1020 V/cm for color superconducting strange matter [37,38]. In [39-49], the impact of ultra-high electric field energy densities on compact star bulk characteristics was investigated.

It has also been demonstrated that, depending on their strength, electric fields of this size, which are produced by charge distributions close to odd stars' surfaces, can raise the stellar mass by as much as 30%. These characteristics might make it possible to observe and differentiate between neutron stars and odd stars. Malaver et al. have conducted studies of compact stars with Buchdahl potential in 5-D Einstein-Gauss-Bonnet gravity and scalar field theory with Buchdahl space-time [43,44]. These researchers have also investigated dark energy stars in Tolman Spacetime and compact stars using Chaplygin Equation of State [45,46].

Numerous studies, including those by Ponce de León, Patel and Vaidya, Tikekar and Thomas [51], Mak and Harko, Chaisi and Maharaj, Maharaj and Chaisi, Sharma and Maharaj, Varela et al., Komathiraj and Maharaj, Takisa and Maharaj, Maharaj and Takisa, Feroze and Siddique, Feroze, Feroze and Tariq, Bhar et al., Murad, and Malaver have created analytical models of strange stars that are mathematically accurate [50-72]. For this reason, ansatz new paradigm PHYSICS has been developed to formalisms that have sound logic with assumption-free theoretical advancements and the ability to be gaged from the quantum to astrophysics regime metrically [74-78]. We would also like to point out that novel paradigm PHYSICS requires an understanding of what is happening inside these galaxies and stars, especially those that are anisotropic, as they may hold clues to the quantum nature [73]. Additionally, Bhar and Murad use a specific kind of metric function to examine a Chaplygin equation of state with a locally anisotropic matter distribution [79]. Our compilation of theoretical and experimental knowledge was recently shown by extensive research with the summary book of Magnetars and Stellar Objects [78].

The conversion of time wavefunction to vector time interacting with gravitational gradient arising in geodesics actual matter spacetime has been explored by Iyer [80]. This led to the theoretical deduction that the astrophysical field may include a domain of reality with a curved time and space-sense confinement that reaches into infinite emptiness. Furthermore, it was discovered theoretically that the rank of tensors is essential for defining various reality domains. Higher rank tensors, for instance, may be the main cause of the faster than light speed in the quantum domain, where instantaneity forces the wavefunction to collapse to equivalent scalar parametric metric fields. Since gravity is a more confined phenomenon that results from the curvature of spacetime to have a unidirectional impact, metrics that affect the gravitational gradient are distinct from those that are affected by the Hamiltonian (activity) via the Rank6 time tensor per algorithm in the immediate past. According to key knowledge, cosmic scale phenomena will often have strong inertial mass and weak gravitational mass, with relativistic effects taking center stage. CMBR (cosmic microwave background radiation) temperature fluctuations, which are brought on by density and velocity perturbations in the early cosmos, are typically represented by the signal's intensity [81].

It has been theoretically demonstrated by Iyer that knowledge of reference frames is essential for conducting physical measurements that measure how our understanding of the cosmos is being shaped [82–83]. Analyzing signal/noise would be crucial physics in this regard, describing quantifiable observables that are developed from abstract theoretical physics towards experimental instrumental design and possible mesoscopic observations with empirical support. In particular, the fundamental nature of signal observables inside many worlds spacetime domains of reality and their behavior at extreme temperatures would be revealed by ansatz signal analysis techniques such as the M-Branes Theory relating signal/noise equivalency of the energy-temperature [84–87].

In this work, we constructed new models for charged anisotropic matter by considering a Bose-Einstein equation of state and a modified form of the gravitational potential proposed by Korkina and Orlyanskii [88,89]. The article is organized as follows: In section 2, we present Einstein's field equations for the distribution of anisotropic fluids. In section 3, by choosing a particular gravitational potential and electric field intensity that allow the field equations to be solved, we construct new models for charged anisotropic matter. Section 4 discusses physical acceptability requirements. The validity and physical properties of these new solutions are examined in Section 5. The conclusions derived from the results of the computational implementations are presented in Section 6.

Equations for Einstein-Maxwell Fields

We consider a spherically symmetric, homogeneous, static spacetime. In Schwarzschild coordinates, the metric is given by

$$ds^2 = -e^{2\nu(r)}dt^2 + e^{2\lambda(r)}dr^2 + r^2(d\theta^2 + \sin^2\theta d\varphi^2) \quad (1)$$

where $\nu(r)$ and $\lambda(r)$ are two arbitrary functions.

The charged anisotropic matter's Einstein field equations are provided by

$$\frac{1}{r^2}\left(1-e^{-2\lambda}\right)+\frac{2\lambda'}{r}e^{-2\lambda} = \rho + \frac{1}{2}E^2 \quad (2)$$

$$-\frac{1}{r^2}\left(1-e^{-2\lambda}\right)+\frac{2\nu'}{r}e^{-2\lambda} = p_r - \frac{1}{2}E^2 \quad (3)$$

$$e^{-2\lambda}\left(\nu''+\nu'^2+\frac{\nu'}{r}-\nu'\lambda'-\frac{\lambda'}{r}\right) = p_t + \frac{1}{2}E^2 \quad (4)$$

$$\sigma = \frac{1}{r^2}e^{-\lambda}(r^2E)' \quad (5)$$

where ρ is the energy density, p_r is the radial pressure, E is electric field intensity, p_t is the tangential pressure and primes denote differentiations with respect to r. Using the transformations, $x = Cr^2$, $Z(x) = e^{-2\lambda(r)}$ and $A^2y^2(x) = e^{2\nu(r)}$ with arbitrary constants A and c>0, suggested by Durgapal and Bannerji [90], the Einstein field equations can be written as

$$\frac{1-Z}{x} - 2\dot{Z} = \frac{\rho}{C} + \frac{E^2}{2C} \quad (6)$$

$$4Z\frac{\dot{y}}{y} - \frac{1-Z}{x} = \frac{p_r}{C} - \frac{E^2}{2C} \quad (7)$$

$$4xZ\frac{\ddot{y}}{y} + (4Z + 2x\dot{Z})\frac{\dot{y}}{y} + \dot{Z} = \frac{p_t}{C} + \frac{E^2}{2C} \quad (8)$$

$$p_t = p_r + \Delta \quad (9)$$

$$\frac{\Delta}{C}=4xZ\frac{\ddot{y}}{y}+\dot{Z}\left(1+2x\frac{\dot{y}}{y}\right)+\frac{1-Z}{x}-\frac{E^2}{C} \quad (10)$$

$$\sigma^2=\frac{4cZ}{x}\left(x\dot{E}+E\right)^2 \quad (11)$$

σ is the charge density, $\Delta = p_t - p_r$ is the anisotropic factor and dots denote differentiation with respect to x. With the transformations of [90], the mass within a radius r of the sphere takes the form

$$m(x)=\frac{1}{4C^{3/2}}\int_0^x \sqrt{x}\left(\rho^*+E^2\right)dx$$

$$\text{where} \quad \rho^*=\left(\frac{1-Z}{x}-2\dot{Z}\right)C$$

The outside spacetime defined by the Reissner-Nordstrom metric should coincide with the internal metric (1) with the charged matter distribution given by

$$ds^2=-\left(1-\frac{2M}{r}+\frac{Q^2}{r^2}\right)dt^2+\left(1-\frac{2M}{r}+\frac{Q^2}{r^2}\right)^{-1}dr^2+r^2(d\theta^2+\sin^2\theta d\varphi^2) \quad (13)$$

where the total mass and the total charge of the star are denoted by M and Q^2, respectively. The junction conditions at the stellar surface are obtained by matching the first and the second fundamental forms for the interior metric (1) and the exterior metric (13). In order to relate the radial pressure to the energy density, where α is a positive constant, we imposed the following quadratic equation of state, also known as the Bose-Einstein equation of state [88].

$$p_r=\alpha\rho^2 \quad (14)$$

Novel Model Classifications

In this study, we selected particular forms for the electric field intensity E and the gravitational potential $Z(x)$ in order to solve the Einstein-Maxwell field equations. In accordance with Korkina and Orlyanskii [89], we decide on $Z(x)$.

$$Z(x)=\frac{1+ax}{1+2ax} \quad (15)$$

a is a real constant in this case. This potential behaves well inside the sphere and is regular at the star center. We use the form suggested by Lighuda et al. [91] for the electric field intensity, which can be expressed as

$$\frac{E^2}{2C}=KxZ(x)=Kx\left(\frac{1+ax}{1+2ax}\right) \quad (16)$$

with $K > 0$. This type of electric field provides us with a positive, continuous, monotonically growing function that is regular at the center of the star.

By changing (15) and (16) in equation (6), we get

$$\rho=C\frac{\left|3a+2a^2x-Kx(1+ax)(1+2ax)\right|}{(1+2ax)^2} \quad (17)$$

By substituting (17) into (14), we obtain the radial pressure

$$P_r=\alpha C^2\frac{\left|3a+2a^2x-Kx(1+ax)(1+2ax)\right|^2}{(1+2ax)^4} \quad (18)$$

The charge density in (11), with (15) and (16), is

$$\sigma^2=\frac{2C^2K\left(3+8ax+6a^2x^2\right)^2}{(1+2ax)^4} \quad (19)$$

The mass function is expressed using (17) in (12).

$$M(x)=\frac{\sqrt{x}}{4\sqrt{C}}\left[\frac{-12Ka^2x^2-10Kax+60a^2+15K}{60a^2}-\frac{1}{2ax+1}\right]-$$

$$\frac{\sqrt{2K}\arctan\left(\sqrt{2ax}\right)}{32a^2\sqrt{aC}} \quad (20)$$

Equation (7) is changed by (15), (16), and (17) as

$$\frac{4(1+ax)}{(1+2ax)}\frac{\dot{y}}{y}=\frac{\alpha c\left[3a+2a^2x-Kx(1+ax)(1+2ax)\right]^2}{(1+2ax)^4}-\frac{Kx(1+ax)}{1+2ax}+\frac{a}{1+2ax} \quad (21)$$

When we integrate (21), we get

$$y(x)=C_1(ax+1)^{A*}(2ax+1)^B e^{\frac{C*x^5+Dx^4+Ex^3+Fx^2+Gx+H}{96(2ax+1)^2}} \quad (22)$$

where

$$A*=-\frac{1}{4}\alpha aC+\frac{1}{4} \quad (23)$$

$$B=\frac{\alpha C\left(16a^4-8Ka^2+K^2\right)}{64a^3} \quad (24)$$

$$C*=16K^2a^2\alpha c \quad (25)$$

$$D=28K^2a\alpha c-48Ka^2 \quad (26)$$

$$E=-96Ka^2\alpha c+4K^2\alpha c-48Ka \quad (27)$$

$$F=\frac{-96Ka^2\alpha c-9K^2\alpha c-12Ka}{a} \quad (28)$$

$$G = \frac{-72Ka^2\alpha c - 3K^2\alpha c}{a^2} \tag{29}$$

$$H = \frac{-48a^2\alpha c - 24K\alpha c}{a} \tag{30}$$

It is possible to express the metric functions as

$$e^{2\lambda(r)} = \frac{1+2ax}{1+ax} \tag{31}$$

$$e^{2\nu(r)} = A^2C_1^{\,2}(ax+1)^{2A^*}(2ax+1)^{2B}\, e^{\frac{C^*x^5+Dx^4+Ex^3+Fx^2+Gx+H}{48(2ax+1)^2}} \tag{32}$$

For the anisotropy Δ is provided

$$\Delta = 4xC\left(\frac{1+ax}{1+2ax}\right)\left\{\begin{aligned}&\frac{(A^{*2}-A^*)a^2}{(ax+1)^2}+\frac{4A^*a^2B}{(ax+1)(2ax+1)}+\\ &\frac{2aA^*}{ax+1}\left[\frac{5C^*x^4+4Dx^3+3Ex^2+2Fx+G}{96(2ax+1)^2}-\frac{a(C^*x^5+Dx^4+Ex^3+Fx^2+Gx+H)}{24(2ax+1)^3}\right]\\ &\frac{4(B^2-B)a^2}{(2ax+1)^2}+\frac{4aB}{2ax+1}\left[\frac{5C^*x^4+4Dx^3+3Ex^2+2Fx+G}{96(2ax+1)^2}-\frac{a(C^*x^5+Dx^4+Ex^3+Fx^2+Gx+H)}{24(2ax+1)^3}\right]\\ &+\frac{20C^*x^3+12Dx^2+6Ex+2F}{96(2ax+1)^2}\\ &-\frac{a(5C^*x^4+4Dx^3+3Ex^2+2Fx+G)}{12(2ax+1)^3}\\ &+\frac{a^2(C^*x^5+Dx^4+Ex^3+Fx^2+Gx+H)}{4(2ax+1)^4}\\ &+\left[\frac{5C^*x^4+4Dx^3+3Ex^2+2Fx+G}{96(2ax+1)^2}-\frac{a(C^*x^5+Dx^4+Ex^3+Fx^2+Gx+H)}{24(2ax+1)^3}\right]^2\end{aligned}\right\}$$
$$-\frac{a}{(1+2ax)^2}\left\{1+2x\left[\frac{A^*a}{ax+1}+\frac{2aB}{2ax+1}+\frac{5C^*x^4+4Dx^3+3Ex^2+2Fx+G}{96(2ax+1)^2}-\frac{a(C^*x^5+Dx^4+Ex^3+Fx^2+Gx+H)}{24(2ax+1)^3}\right]\right\}+\frac{a}{1+2ax}$$
$$-\frac{2Kx(1+ax)}{1+2ax} \tag{33}$$

Physical Acceptability Requirements

A model must meet the following requirements in order to be considered physically acceptable [29,92]:

(i) The metric potentials $e^{2\lambda}$ and $e^{2\nu}$ assume finite values throughout the stellar interior and are singularity-free at the center r=0.

(ii) The energy density ρ inside the star should be positive and decreasing.

(iii) The radial pressure should also be positive and decrease as the radial parameter increases.

(iv) The gradients in radial pressure and density

$dp_r/dr \le 0$ and $d\rho/dr \le 0$ for $0 \le r \le R$. (v)

At the center, the anisotropy is zero r=0, i.e. $\Delta(r=0)=0$.

(vi) The causality requirement, which states that the radial speed of sound v_{sr}^2 must be less than the speed of light throughout the model, must be met by any physically feasible solution, i.e.

$$0 \le v_{sr}^2 = \frac{dp_r}{d\rho} \le 1.$$

The Reissner-Nordstrom spacetime's exterior and the interior solution should coincide; the metric for this is

$$ds^2 = -\left(1-\frac{2M}{r}+\frac{Q^2}{r^2}\right)dt^2 + \left(1-\frac{2M}{r}+\frac{Q^2}{r^2}\right)^{-1} dr^2 + r^2d\theta^2 + r^2\sin^2\theta d\varphi^2$$

through the boundary $r=R$ where M and Q are the total mass and the total charge of the star, respectively.

According to criteria (ii) and (iv), the energy density must be at its highest at the center of the sphere and decrease as it moves toward the surface.

Physical Examination of the Novel Models

Metric potentials for the new solutions $e^{2\lambda}$ and $e^{2\nu}$ have limited quantities and maintain a positive value throughout the interior of the star. At the center $e^{2\lambda(0)} = 1$ and $e^{2\nu(0)} = A^2C_1^2e^{\frac{H}{48}}$. We show that in $r=0$ $\left(e^{2\lambda(r)}\right)'_{r=0} = \left(e^{2\nu(r)}\right)'_{r=0} = 0$ and this enables the confirmation of the regularity of the gravitational potentials at the center. Between the star's core and surface, the energy density is positive and behaves well.

In the center $\rho(r=0) = 3aC$ and $P_r(r=0) = 9\alpha a^2C^2$ Consequently, the energy density won't be negative in r=0 and $P_r(r=0) > 0$. On the star's surface and additionally, for the second fundamental form, we have

$$3a + 2a^2CR^2 - KCR^2(1+aCR^2)(1+2aCR^2) = 0 \tag{34}$$

Radial pressure gradients and energy density $\frac{d\rho}{dr}$ and $\frac{dP_r}{dr}$ are functions that decrease monotonically with the radial coordinate r, respectively. In this instance, we get in

$$\frac{d\rho}{dr}=\frac{\left[C\left((4a^2Cr-2KCr(1+aCr^2)(1+2aCr^2)-2aKC^2r^3(1+2aCr^2)-4aKC^2r^3(1+aCr^2)\right)\right]}{\left(1+2aCr^2\right)^2}-\frac{8arC^2\left[3a+2a^2Cr^2-KCr^2\left(1+aCr^2\right)\left(1+2aCr^2\right)\right]}{\left(1+2aCr^2\right)^3}\leq 0 \quad (35)$$

$$\frac{dP_r}{dr}=\frac{\left[\begin{array}{l}\left(2\alpha C^2(3a+2a^2Cr^2-KCr^2(1+aCr^2)(1+2aCr^2)\right)\\ \left(4a^2Cr-2KCr(1+aCr^2)(1+2aCr^2)-2aKC^2r^3(1+2aCr^2)-4aKC^2r^3(1+aCr^2)\right)\end{array}\right]}{\left(1+2aCr^2\right)^4}-\frac{16a\alpha rC^3\left(3a+2a^2Cr^2-KCr^2(1+aCr^2)(1+2aCr^2)\right)^2}{\left(1+2aCr^2\right)^5}\leq 0 \quad (36)$$

It may be inferred from equations (35) and (36) that the pressure and density should be highest in the star's center and monotonically decrease toward its surface. The radial sound speed must remain within the limit in order to maintain causality $0 \leq v_{sr}^2 \leq 1$ within the star's interior [92]. This model includes:

$$0\leq v_{sr}^2=\frac{dp_r}{d\rho}=2\alpha C\frac{\left[3a+2a^2Cr^2-KCr^2\left(1+aCr^2\right)\left(1+2aCr^2\right)\right]}{\left(1+aCr^2\right)^2}\leq 1 \quad (37)$$

On the edge $r=R$, the solution must match the Reissner–Nordström exterior space–time and the continuity of e^{ν} and e^{λ} across the boundary $r=R$ is

$$e^{2\nu}=e^{-2\lambda}=1-\frac{2M}{R}+\frac{Q^2}{R^2} \quad (38)$$

Next, we get the following for the matching conditions:

$$\frac{2M}{R}=\frac{aCR^2+2C^2R^4+2aC^3R^6}{1+2aCR^2} \quad (39)$$

The masses of the star objects and the values of the selected physical parameters, α, a, and K, are displayed in Table 1.

Table 1: Parameters K, a, α and stellar masses.

K	α	a	$M(M_{\Theta})$
0.0000101	1/3	0.015	1.159730526
0.0000105	1/3	0.015	1.159033690
0.0000111	1/3	0.015	1.157988440

M_{Θ} = sun's mass

The figures 1,2,3,4,5,6,7,8, 9,10 and 11 represent the plots of $e^{2\lambda}$, $e^{2\nu}$, $\frac{E^2}{2C}$, σ^2, ρ, P_r, v_{sr}^2, $\frac{d\rho}{dr}$, $\frac{dP_r}{dr}$, Δ and M with the radial coordinate. In every graph we looked at C=1.

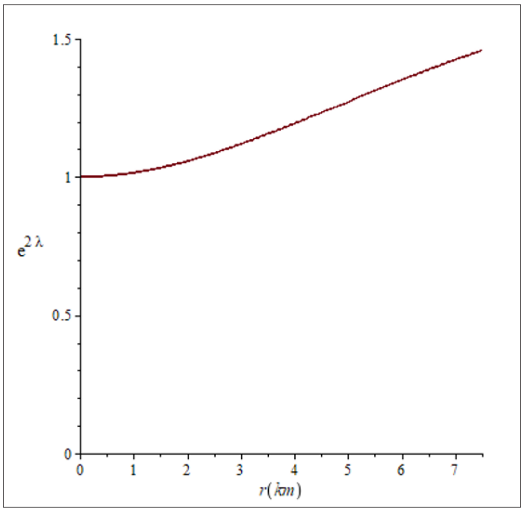

Figure 1: Potential metric $e^{2\lambda}$ in opposition to the radial coordinate for a=0.015.

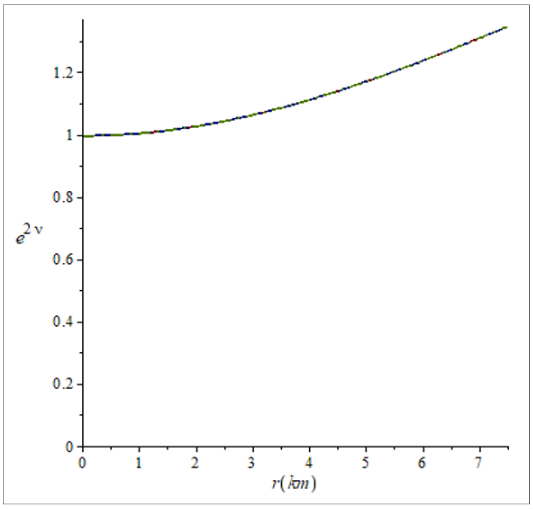

Figure 2: Potential metric $e^{2\nu}$ in opposition to the radial parameter. For all the cases a=0.015. Here, solid, long-dash and dot-dashed lines correspond to K= 0.0000101, 0.0000105 and 0.0000111 respectively

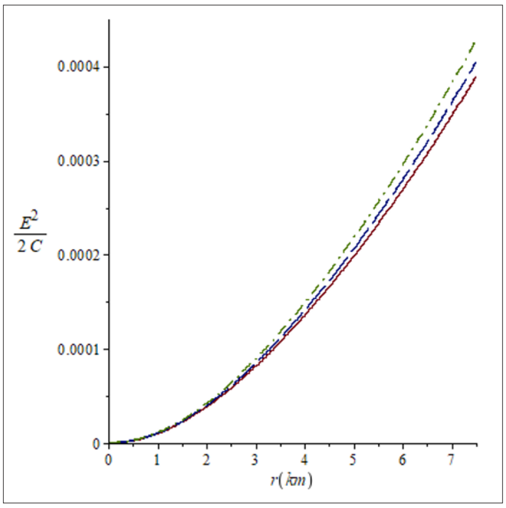

Figure 3: Against the radial coordinate, an electric field for K=0.0000101 (solid line), K=0.0000105 (long- dash line) and K=0.0000111 (dash-dot line). For all the cases a=0.015.

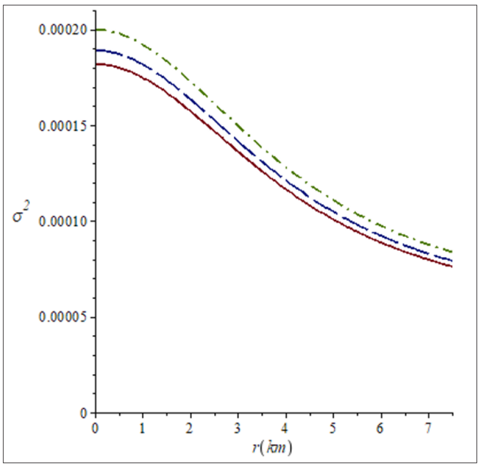

Figure 4: Charge density in opposition to the radial parameter for K=0.0000101 (solid line), K=0.0000105 (long- dash line) and K=0.0000111 (dash-dot line). For all the cases a=0.015.

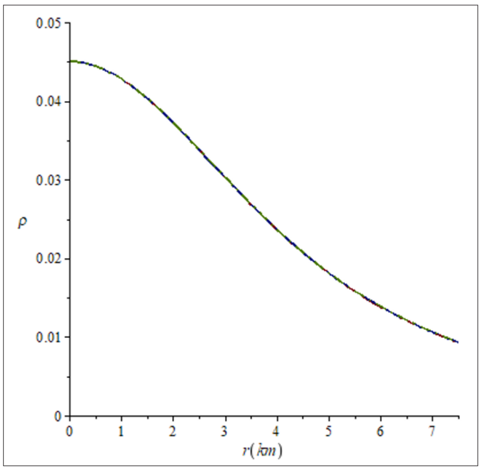

Figure 5: Energy density ρ against the radial coordinate. For all the cases a=0.015. Here, solid, long-dash and dot-dashed lines correspond to K= 0.0000101, 0.0000105 and 0.0000111 respectively

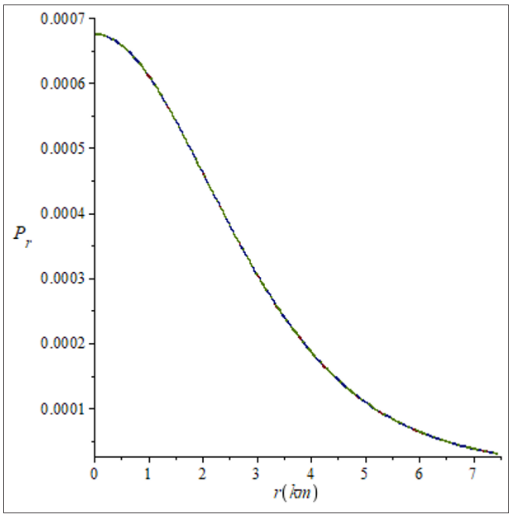

Figure 6: Radial pressure P_r against the radial coordinate. For all the cases a=0.015. Here, solid, long-dash and dot-dashed lines correspond to K= 0.0000101, 0.0000105 and 0.0000111 respectively

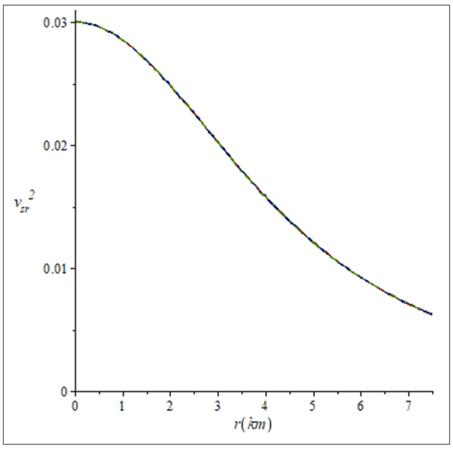

Figure 7: Radial speed sound v_{sr}^2 against the radial coordinate.

For all the cases a=0.015. Here, solid, long-dash and dot-dashed lines correspond to K= 0.0000101, 0.0000105 and 0.0000111 respectively

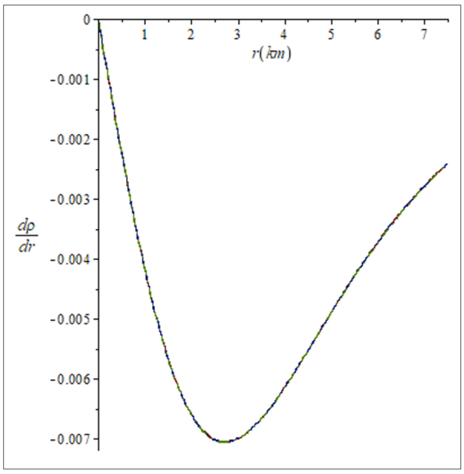

Figure 8: Gradient of energy density versus the radial coordinate. For all the cases a=0.015. Here, solid, long-dash and dot-dashed lines correspond to K= 0.0000101, 0.0000105 and 0.0000111 respectively.

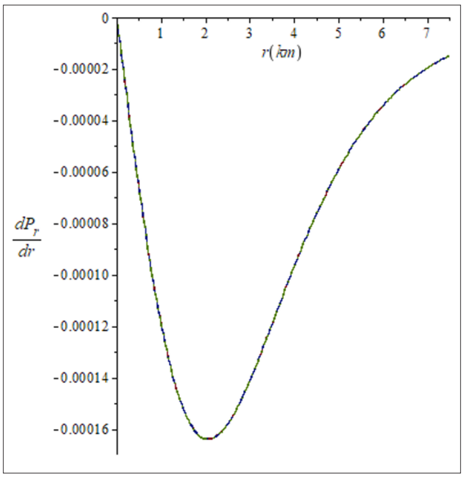

Figure 9: Gradient of radial pressure versus the radial parameter. For all the cases a=0.015. Here, solid, long-dash and dot-dashed lines correspond to K= 0.0000101, 0.0000105 and 0.0000111 respectively

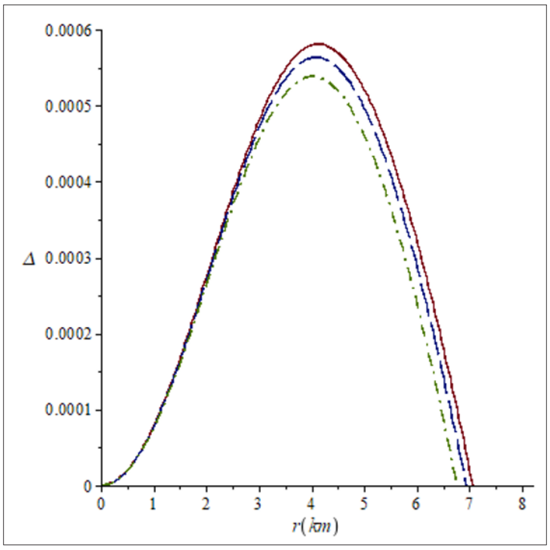

Figure 10: Anisotropy against the radial parameter. For all the cases a=0.015. Here, solid, long-dash and dot-dashed lines correspond to K= 0.0000101, 0.0000105 and 0.0000111 respectively

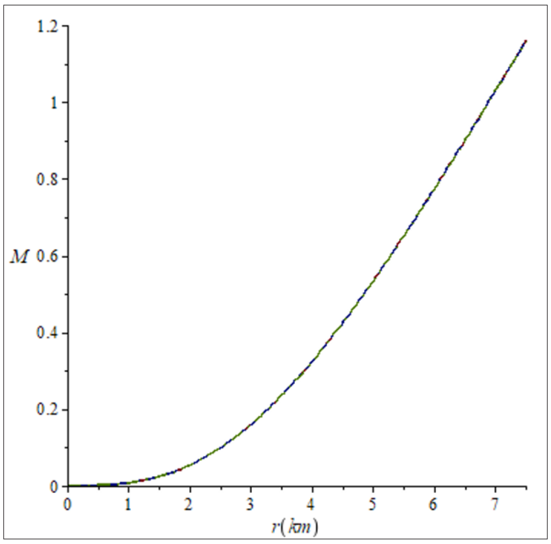

Figure 11: Mass function against the radial coordinate. For all the cases a=0.015. Here, solid, long-dash and dot-dashed lines correspond to K= 0.0000101, 0.0000105 and 0.0000111 respectively

In Figure 1, The potential metric $e^{2\lambda}$ is a function that grows steadily inside the star and increases in value with the radial parameter. In Figure 2, the metric potential also is continuous and has the same behaviour as that of $e^{2\lambda}$, achieving high radial parameter values. Figure 3 shows that for all values of K taken into consideration, the electric field intensity stays positive, continuous, and increases monotonically throughout the star interior. As seen in Figure 4, the charge density is a function that decreases steadily. Figure 5 illustrates that the star's internal energy density is continuous and decreases monotonically, whereas Figure 6 shows that the radial pressure is non-negative and decreases with the radial parameter. In Figure 7 the profile of radial speed sound is plotted with radial parameter and is noted that v_{sr}^2 as demonstrated by Delgaty and Lake, is always less than the unity and causality condition that is maintained in the star interior, which is a crucial physical need [29]. The radial variation of energy density gradient has been shown in Figure 8, in which it is observed that $\frac{d\rho}{dr} < 0$ in all the cases studied. In Figure 9 it is also shown that the profile $\frac{dP_r}{dr}$ of indicates the radial pressure gradient is negative inside the star. Plotting the anisotropic component Δ in Figure 10 reveals that it disappears at the star's center, or Δ(r=0)=0. Additionally, we may observe that as K increases, Δ admits smaller values. For a range of K values, the mass function in Figure 11 is continuous, rising, takes finite values, and behaves nicely in the star interior. The estimated values can be compared to the stellar masses of the three celestial objects in Table 2 [93,94].

Table 2: The approximate values of the masses for the compact stars

Compact Star	Masses $M(M_\Theta)$
GW191219	1.17
J1741+1351	1.14
4FGLJ2039.5-5617	1.18

The masses produced by the selected values of the parameter *K* are extremely similar to the binary system GW191219 [93], which consists of a black hole and neutron star. The behavior of the star's mass, electric field *E*, and charge density with the radial parameter at a value of *K* = 0.0000101 is displayed in Table 3. The electric field strength *E* and charge density *σ* are finite and nonsingular across the star where *E*=0 at *r*=0, and the mass function increases as r increases.

Table 3: Variation of Mass *M*, electric field E^2 and charge density σ^2 with *K*=0.0000101 and *a*=0.015 from centre to the surface of the star

r	*M*	E^2 /2C	σ^2
0	0	0	0.0001818
1	0.0072805540	0.000009952912621	0.0001749
2	0.0535403760	0.000038235714290	0.0001574
3	0.1592229801	0.000081237401570	0.0001363
4	0.3234197170	0.000135394594600	0.0001167
5	0.5330961708	0.000198392857100	0.0001009
6	0.7726592458	0.000269203846200	0.0000888
7.5	1.1597305260	0.000389760174500	0.0000761

The values found in this study using the Bose-Einstein equation of state for the mass, charge, and electric field for the black hole-neutron star binary system corresponding to GW191219 [93] are regular and behave well in the stellar interior.

LIGO measurements of gravitational waves from a binary black hole merger [85] and the dynamics of neutron star mergers, which result in the emission of gravitational waves indicating the potential formation of heavy elements, can both be predicted by simulations, particularly when numerical relativity is used. As shown in the work of Müller and Rezzolla and Gonzalez et al., advanced simulations using numerical relativity may potentially explore phenomena such as unusual stars, wormholes, and quantum gravity effects in strong gravitational fields [86,87].

In order to advance the timeline, Iyer's work [80], which was first mentioned in the Introduction, theoretically demonstrates that the gravitational gradient that twists the tensor time will depend on the immediate future of the action that formed the time wavefunction. Here, Iyer has demonstrated that the classical scalar equation of motion under gravitational fields can be obtained by interactively coupling gravity-time metrics to determine action Lagrange in general scalar time and scalar gravity. The Lagrangian of action S = ∫L dt, with L = f (mwg, tqg, R), with R = scalar 4D toroidal hyperspace coupling, interactively linking with scalar gravitational mass mwg and scalar quantum gravity time tqg operator with gravitational fields. Importantly, astrophysical regions would exhibit a rank2 tensor, which is analogous to Schwarzschild metrics and would correspond to what we know about Schwarzschild metrics solving general relativity formulations, as demonstrated in the current work results discussed above. These sophisticated theoretical derivations helped to conjecture that, in terms of rank gradation of tensors, quantum domains cause fields polarization to the rank6 tensor time, while mesoscopic environments would manifest rank mixing 2 and 4. Because quantum gravitational effects are important during the Planck era, tensor gradation to scalar metrics can therefore offer fresh perspectives on the behavior of the early universe's cosmology and astrophysics. This could lead to more accurate models of the Big Bang and subsequent cosmic evolution. The discrete nature of spacetime suggested by tensor gradation might offer new perspectives on black hole entropy and information paradoxes, potentially leading to a deeper understanding of black hole thermodynamics [80].

The causation of polarization exhibiting CMBR anisotropy is based on the Thomson scattering of light by free electrons in the final scattering surface. Using the "ket" matrix and bra matrix with six vector time elements and two scalar time elements, Iyer's research demonstrates a rank-6 tensor time matrix that is useful for testing the parameters of various cosmological models, including inflation, dark matter, dark energy, and neutrino masses. This research typically aids in measuring the global and local clocking time-value of events as listed by all of these phenomena, some of which have been extensively considered in this article, building on the Introduction literature survey [81].

The significance of perfectly accurate reference frames determined theoretically towards Global Positioning System, Laser Interferometer Gravitational-Wave Observatory data has just been reported by Iyer, as well as well stated by Introduction studies [82]. For example, (1) time measurements require weak-gravity reference frames because gravitational fields affect time, particularly when they are close to massive objects or fluctuating gravitational potentials; (2) mass measurements are best performed in a zero-gravity reference frame because gravitational forces can alter an object's apparent weight and impact the measurement of mass. Relativity-based calibration is required for accurate time measurements. Accurate mass measurement is ensured in a zero-gravity environment, free from outside gravitational forces; (3) refining early universe models by examining cosmic phenomena including black hole dynamics and the cosmic microwave background (CMB); (4) increasing the sensitivity and precision of gravitational wave detectors, like LIGO, to better detect weak signals from astrophysical events.

Iyer's research on quantum cosmology has revealed measurable observables that limit the temporal and spatial dimensions of existence [83]. The M-Branes Theory, which links the signal/noise equivalence of the energy-temperature advances mathematical algorithm equations configurationally describing signal/noise behavior at various domains of spacetime reality, is a further development of the thesis. In order to explain the evolution of diffused quantum state ensembles physical states, such as open strings, which characterize CMBR longitudinal waves, in contrast to the closed strings that characterize gravitational transverse waves on curved or curled up dimensional branes, this would also extend to the idea of Planck Boltzmann branes separated by discontinuum length, DL.

The mathematics of end states of universal existence is magically defined by the transformation of the signal variance to temperature variance; for instance, the universe tends toward a vacuum state at high infinite temperatures and becomes superconductive at absolute zero. In order to quantitatively characterize the graviton as a quantum microblackhole, Iyer's physics department develops an experimental method of Spin Spectroscopy signal/noise algorithm to theoretically measure particle mass, charge, microsymmetry in quantum, and macrosymmetry within crystal structures. This will be proven with LHC and particle accelerator measurements, which will contribute to the validity of M Branes Theories' Quantum Gravity Grand Unified PHYSICS [83].

Conclusion

In this study, we created a few basic relativistic charged star models for a static spherically symmetric locally anisotropic fluid distribution by solving Einstein-Maxwell field equations. We have examined the behavior of fluid distribution by selecting a metric potential, calculating the electric charge distribution, and using the Bose-Einstein equation of state. The explanation of the internal structure of electrically charged odd stars may benefit greatly by an analytical stellar model with such physical characteristics. Since matter variables and the gravitational potentials of this study are compatible with the physical analysis of these stars, the newly discovered models align seamlessly with the Schwarzschild exterior metric across the boundary r=R.

Plots produced and physical characteristics related to matter, radial pressure, density, anisotropy, and charge density indicate that the suggested model behaves well and may be compared to the binary system GW191219. Simulations, especially with numerical relativity can predict binary black hole mergers causing gravitational waves as well as the dynamics of mergers of neutron stars, causing emission of gravitational waves pointing to possible formation of heavy elements, wormholes, exotic stars, and quantum gravity effects in strong gravitational fields.

A new ansatz understanding of nature of time as a rank6 tensor that degrades to vector to entangle with gravitational gradient creating real matter universe has been also highlighted here. Measurements, reference frames, end states of the universe, as well as abstract signal algorithmic transformation to interpret faint signals and thermodynamics have been explicably summarized here in this quantum Bose-Einstein condensate with cosmological Modelling of a neutron star-black hole system.

References

1. Kuhfitting PK (2011) Some remarks on exact wormhole solutions, Adv Stud Theor Phys 5: 365-367
2. Bicak J (2006) Einstein equations: exact solutions, Encyclopedia of Mathematical Physics 2: 165-173.
3. Schwarzschild K (1916) Über das Gravitationsfeld einer Kugel aus inkompressibler Flussigkeit nach der Einsteinschen Theorie. Math Phys Technol 424-434.
4. Einstein A (1917) Cosmological Considerations in the General Theory of Relativity. Preus Akad Wissen Sitz 142: 487.
5. Ivanov BV (2017) Analytical study of anisotropic compact star models. Eur Phys JC 77: 738.
6. Ruderman RA (1972) Pulsars: structure and dynamics. Rev Astr Astrophys 10: 427.
7. Canuto V (1973) Neutron Stars: General Review Solvay Conference on Astrophysics and Gravitation Brussels.
8. Dev K, Gleiser M (2002) Anisotropic Stars: Exact Solutions. Gen Rel Grav 34: 1793.
9. Sokolov AI (1980) Phase transitions in a superfluid neutron liquid. Sov Phys JETP 52: 575.
10. Usov VV (2004) Electric fields at the quark surface of strange stars in the color-flavor locked phase. Phys Rev 70: 067301.
11. Bowers RL, Liang EPT (1974) Anisotropic Spheres in General Relativity. Astrophys J 188: 657-665.
12. Cosenza M, Herrera L, Esculpi M, Witten L (1982) Evolution of radiating anisotropic spheres in general relativity. Phys Rev 25: 2527-2535.
13. Bayin SS (1982) Anisotropic fluid spheres in general relativity. Phys Rev 26: 1262.
14. Krori KD, Borgohaiann P, Devi R (1984) Some exact anisotropic solutions in general relativity. Can J Phys 62: 239.
15. Herrera L, Ponce de León J (1985) Isotropic and anisotropic charged spheres admitting a one-parameter group of conformal motions J Math Phys 26.
16. Ponce de León J (1987) General relativistic electromagnetic mass models of neutral spherically symmetric systems. Gen Relat Grav 19: 797.
17. Ponce de León J (1987) New analytical models for anisotropic spheres in general Relativity. J Math Phys 28: 1114.
18. Bondi H (1992) Anisotropic spheres in general relativity. Mon Not R Astron Soc 259: 365.
19. Herrera L, Santos, N (1997) Local anisotropy in self-gravitating systems. Phys Rep 286: 53.
20. Herrera L, Prisco, AD, Ospino J (2001) Fuenmayor. E. Conformally flat anisotropic spheres in general relativity. J Math Phys 42: 2129.
21. Herrera L, Ospino J, Prisco AD (2008) All static spherically symmetric anisotropic solutions of Einstein´s equations. Phys Rev 77: 027502.
22. Dev K, Gleiser M (2003) Anisotropic Stars II: Stability. Gen Relativ Gravit 35: 1435-1457.
23. Ivanov BV (2010) The Importance of Anisotropy for Relativistic Fluids with Spherical Symmetry. Int J Theor Phys 49: 1236-1243.
24. Ivanov BV (2002) Maximum bounds on the surface redshift of anisotropic stars Phys Rev 65: 104011.
25. Mak MK, Harko T (2002) An exact Anisotropic Quark Star Model. Chin J Astron Astrophys 2: 248.
26. Mak MK, Harko T (2003) Anisotropic Stars in General Relativity. Proc R Soc Lond 459: 393
27. Mak MK, Dobson PN, Harko T (2002) Exact models for anisotropic relativistic stars. Int J Mod Phys 11: 207-221.
28. Viaggiu S (2009) Modeling usual and unusual anisotropic spheres. Int J Mod Phys 18: 275.
29. Malaver M (2014) Strange Quark Star Model with Quadratic Equation of State. Frontiers of Mathematics and Its Applications 1: 9-15.
30. Malaver M (2014) Quark star model with charge distribution. Open Science Journal of Modern Physics 1: 6-11.
31. Malaver M (2016) Classes of relativistic stars with quadratic equation of state. World Scientific News 57: 70-80.
32. Malaver M (2013) Analytical model for charged polytropic stars with Van der Waals equation of state. American Journal

of Astronomy and Astrophysics 1: 41-46.
33. Malaver M (2013) Regular model for a quark star with Van der Waals modified equation of State. World Applied Programming 3: 309-313.
34. Malaver M (2015) Relativistic Modeling of Quark Stars with Tolman IV Type Potential. Int J Modern Physics and Application 2: 1-6.
35. Pant N, Pradhan N, Malaver M (2015) Anisotropic fluids star model in isotropic coordinates. Int J Astrophys Space Sci 3: 1-5.
36. Itoh N (1970) Hydrostatic Equilibrium of Hypothetical Quark Stars. Prog Theor Phys 44: 291.
37. Farhi E, Jaffe RL (1984) Strange matter. Phys Rev D 30: 2379.
38. Usov VV, Harko T, Cheng KS (2005) Structure of the Electrospheres of Bare Strange Stars. Astrophys J 620: 915.
39. Negreiros RP, Mishustin IM, Schramm S, Weber F (2010) Properties of Bare Strange Stars associated with surface electric fields. Phys Rev D 82: 103010.
40. Ray S, Espíndola AL, Malheiro M, Lemos JPS, Zanchin VT (2003) Electrically charged compact stars and formation of charged black holes. Phys Rev D 68: 084004.
41. Malheiro M, Picanco R, Ray S, Lemos JPS, Zanchin VT (2004) Of charged stars and charged black holes. Int J Mod Phys 13: 1375-1379.
42. Weber F, Meixner M, Negreiros RP, Malheiro M (2007) Ultra-dense neutron star matter, strange quark stars and the nuclear equation of state. Int J Mod.Phys 16: 1165-1180.
43. Malaver M, Iyer R, Kar A, Sadhukhan S, Upadhyay S, et al. (2022) Buchdahl Spacetime with Compact Body Solution of Charged Fluid and Scalar Field Theory. General Relativity and Quantum Cosmology. arXiv:2204.00981.
44. Malaver M, Iyer R, Khan I (2022) Study of Compact Stars with Buchdahl Potential in 5-D Einstein-Gauss-Bonnet Gravity. Physical Science International Journal. 26: 1-18.
45. Malaver M, Iyer R (2022) Analytical model of compact star with a new version of modified chaplygin equation of state, Applied Physics 5: 18-36.
46. Malaver M, Iyer R (2024) Modelling of Charged Dark Energy Stars in a Tolman IV Spacetime. Open J of Astronomy 2: 000114.
47. Weber F, Negreiros R, Rosenfield P (2009) Neutron Stars and Pulsars, Astrophysics and Space Science Library 357. https://content.e-bookshelf.de/media/reading/L-12668-0eb2a84126.pdf
48. Weber F, Hamil O, Mimura K, Negreiros RP (2010) From Crust to Core: A brief review of quark matter in neutron stars. Int J Mod Phys D 19: 1427-1436.
49. Negreiros RP, Weber F, Malheiro M, Usov V (2009) Electrically charged strange quark stars. Phys Rev D 80: 083006.
50. Patel LK, Vaidya SK (1996) Anisotropic Fluid spheres in general relativity. Acta Phys Hung Heavy Ion Phys 3: 177.
51. Tikekar R, Thomas VO (1999) Anisotropic fluid distribution on pseudo-spheroidal spacetimes. Pramana J Phys 52: 237.
52. Mak MK, Harko T (2004) Quark stars admitting a one-parameter group of conformal Motions. Int J Mod Phys 13: 149-156.
53. Chaisi M, Maharaj SD (2005) Compact anisotropic spheres with prescribed energy Density. Gen Relativ Gravit 37: 1177-1189.
54. Chaisi M, Maharaj SD (2006) Anisotropic static solutions in modelling highly compact bodies Pramana J Phys 66: 609-614.
55. Chaisi M, Maharaj SD (2006) A new algorithm for anisotropic solutions. Pramana J Phys 66: 313-324.
56. Maharaj SD, Chaisi M (2006) Equation of state for anisotropic spheres. Gen. Relativ Gravit 38: 1723-1726.
57. Maharaj SD, Chaisi M (2006) New anisotropic models from isotropic solutions. Math Meth Appl Sci 29: 67.
58. Sharma R, Maharaj SD (2007) A class of relativistic stars with a linear equation of state. Mon Not R Astron Soc 375: 1265-1268.
59. Varela V, Rahaman F, Ray S, Chakraborty K, Kalam M (2010) Charged anisotropic matter with linear or nonlinear equation of state. Phys Rev D 82: 044052.
60. Komathiraj K, Maharaj SD (2007) Analytical models for quark stars. Int J Mod Phys 16: 1803-1811. 61.
61. Takisa, P.M., Maharaj, S.D. Compact models with regular charge distributions. Astrophys and Space Sci 343: 569-577.
62. Takisa PM, Maharaj SD (2019) Effect of electric charge on conformal compact stars. Eur Phys JC 79: 8.
63. Takisa PM, Maharaj SD (2013) Some charged polytropic models. Gen Relativ Gravit 45: 1951.
64. Takisa PM, Maharaj SD (2012) Regular models with quadratic equation of state. Gen Relativ Gravit 44: 1419-1432.
65. Feroze T, Siddique AA (2011) Charged anisotropic matter with quadratic equation of state. Gen Relativ Gravit 43: 1025-1035.
66. Feroze T, Siddique AA (2014) Some exact solutions of the Einstei-Maxwell equations with a quadratic equation of state. Journal of Korean Physical Society 65: 944-947.
67. Feroze T (2012) Exact solutions of the Einstein-Maxwell equations with linear equation of state. Can J Phys 90: 1179.
68. Feroze T, Tariq H (2014) Exact solutions of the Einstein equations with polytropic equations of state. Can J Phys 93: 637.
69. Bhar P, Murad MH, Pant N (2015)Relativistic anisotropic stellar models with Tolman VII spacetime. Astrophys Space Sci 359: 13.
70. Murad MH (2016) Some analytical models of anisotropic strange stars. Astrophys Space Sci 361: 1-13.
71. Malaver M (2014) Models for quark stars with charged anisotropic matter. Research Journal of Modeling and Simulation. 1: 65-71.
72. Malaver M (2016) New models for charged anisotropic stars with modified Tolman IV spacetime. Int J Modern Physics and Application 3: 6-13.
73. Hossenfelder S (2016) Interpretation of Quantum Field Theories with a Minimal Length Scale, Physical Review D 73: 105013.
74. Taylor E, Iyer R (2022) Rethinking special relativity, spacetime, and proposing a discontinuum. Physics Essays 1: 55-60.
75. Iyer R (2022) Review force general conjectural modeling transforms formalism physics. Physics & Astronomy International Journal 6: 119-124.
76. Iyer R, O'Neill C, Malaver M (2020) Helmholtz Hamiltonian Mechanics Electromagnetic Physics Gaging Charge Fields Having Novel Quantum Circuitry Model. Oriental Journal of Physical Sciences 5: 30-48.
77. Taylor E, Iyer R (2022) Discontinuum physics leads to a table of realities for making predictions. Physics Essays 35: 395-397.
78. Malaver M, Kasmaei H, Iyer R (2022) Magnetars and Stellar Objects: Applications in Astrophysics. Eliva Press Global Ltd., Moldova, Europe: 274.

79. Bhar P, Murad MH (2016) Relativistic compact anisotropic charged stellar models with Chaplygin equation of state. Astrophysics Space Sci 361: 334.
80. Iyer R (2025) Scalar Metrics Tensor Gradation Rank-n Quantum Gravity Physics. Open J of Astro 3: 000155.
81. Iyer R (2024) Quantum Gravity Time Rank-N Tensor Collapsing Expanding Scalar Sense Time Space Matrix Signal/Noise Physics Wavefunction Operator. Phys Sci & Biophys J 8: 000272.
82. Iyer R (2025) Problem Solving Measurement Physics References Entity Calibrational Systems. Oriental Jornal of Physical Sciences 10. https://bit.ly/3PvNxTZ.
83. Iyer R (2024) Signals/Noise Measurable Observables Limiting Temporal Spatial Domains of Reality Defining Physics. Phys Sci & Biophys J 8: 000279.
84. Barausse, E., Morozova, V & Rezzolla, L (2008). On the mass radiated by coalescing black-hole binaries. https://arxiv.org/abs/1206.3803
85. LIGO Scientific Collaboration, Virgo Collaboration (2016) Observation of gravitational waves from a binary black hole merger. Physical Review Letters 116: 061102.
86. Bishop, N., & Rezzolla, L. (2016). Extraction of Gravitational Waves in Numerical Relativity. https://arxiv.org/abs/1606.02532
87. Gonzalez JA (2007) The inspiral and merger of binary black holes: Numerical relativity and gravitational wave observatories. Physical Review D 76: 124022.
88. Chavanis,P.H & Harko, T. https://arxiv.org/abs/1108.3986.
89. Korkina MP, Orlyanskii OY (1991) The Ukrainian Journal of Physics, 36: 885.
90. Durgapal MC, Bannerji R (1983) New analytical stellar model in general relativity. Phys Rev D 27: 328-331.
91. Lighuda AS, Sunzu JM, Maharaj SD, Mureithi EW (2021) Charged stellar model with three layers. Res Astron Astrophys 21: 310.
92. Delgaty MSR, Lake K (1998) Physical Acceptability of Isolated, Static, Spherically Symmetric, Perfect Fluid Solutions of Einstein's Equations. Comput Phys Commun 115: 395.
93. Liu T, Wang Y, Zhao W (2022) Gravitational waveforms from the inspiral of compact binaries in the Brans-Dicke theory in an expanding Universe: 1-20. https://arxiv.org/abs/2205.03704.
94. Fan YZ, Han MZ, Jiang JL, Shao DS, Tang SP (2024) Maximum gravitational mass MTOV=2.25+0.08−0.07M⊙ inferred at about 3% precision with multimessenger data of neutron stars. Phys Rev D 109: 043052.